Biomechanical Profiling of *Caenorhabditis elegans* Motility

Predrag Krajacic,*[,1] Xiaoning Shen,[†,1] Prashant K. Purohit,[†] Paulo Arratia,[†,2] and Todd Lamitina*[,2]
*Department of Physiology and [†]Department of Mechanical Engineering and Applied Mechanics, University of Pennsylvania, Philadelphia, Pennsylvania 19104

ABSTRACT *Caenorhabditis elegans* locomotion is a stereotyped behavior that is ideal for genetic analysis. We integrated video microscopy, image analysis algorithms, and fluid mechanics principles to describe the *C. elegans* swim gait. Quantification of body shapes and external hydrodynamics and model-based estimates of biomechanics reveal that mutants affecting similar biological processes exhibit related patterns of biomechanical differences. Therefore, biomechanical profiling could be useful for predicting the function of previously unstudied motility genes.

REGULATION of motility is a complex biological phenomenon, requiring precise coordination between sensory, motor, and contractile systems. Genetic studies in the nematode *Caenorhabditis elegans* have played a major role in our molecular understanding of these processes. Like other nematodes, *C. elegans* moves by generating waves of dorsal-ventral bends and propagating them along its body from head to tail (for forward locomotion). Major defects in this regular bending wave pattern are easily identified and have led to the isolation of >100 Uncoordinated (Unc) mutants, which affect genes involved in sarcomere structure/function, synapse development and stability, and extracellular matrix formation (Brenner 1974). However, recent studies have revealed that inhibition of genes with major roles in muscle or synapse function does not cause an obvious Unc phenotype (Touroutine *et al.* 2005; Nahabedian *et al.* 2011). This has led to the conclusion that there is significant genetic redundancy in the motor pathway and that more sensitive metrics of motility are needed to fully characterize locomotory phenotypes. Toward this goal, various tracking algorithms and software to monitor nematode swimming have been proposed and built (Pierce-Shimomura *et al.* 2008; Tsechpenakis *et al.* 2008; Buckingham and Sattelle 2009; Fang-Yen *et al.* 2011). While each of these platforms has contributed in a significant way to our understanding of locomotion, a simple, quantitative, and platform-independent tool for measuring multiple parameters of *C. elegans* locomotion is still lacking.

Here, we present an algorithm compatible with most standard digital microscopes that quantifies and integrates various features of the *C. elegans* swim gait. Our method, which we term biomechanical profiling (BMP), integrates non-invasive video microscopy, image analysis algorithms, and fluid mechanics principles to quantify 18 distinct kinematic and biomechanical features of *C. elegans* swimming locomotion. While this platform allows comparisons between each individual feature, we also show that the relative feature pattern is a sensitive phenotypic descriptor. Using BMP, we analyzed 21 well-described mutants affecting two aspects of neuromuscular function: synaptic transmission and sarcomere stability. Unbiased computational clustering of BMP patterns shows that genes with related biological function also have related BMP patterns. As the BMP library of well-characterized mutants expands, this tool will provide a powerful predictor of gene function. The MATLAB codes, sample data, and software tutorial can be freely downloaded from our website (http://www.med.upenn.edu/lamitinalab/downloads) and are available as supporting information, Table S1, File S1, and File S2.

doi: 10.1534/genetics.112.141176
Manuscript received February 10, 2012; accepted for publication April 27, 2012
Supporting information is available online at http://www.genetics.org/content/suppl/2012/05/02/genetics.112.141176.DC1.
[1]These authors contributed equally to this work.
[2]Corresponding authors: Department of Physiology, University of Pennsylvania, Richards Research Bldg. A702, 3700 Hamilton Walk, Philadelphia, PA 19104. E-mail: lamitina@mail.med.upenn.edu; Department of Mechanical Engineering and Applied Mechanics, University of Pennsylvania, Philadelphia, PA 19104. E-mail: parratia@seas.upenn.edu

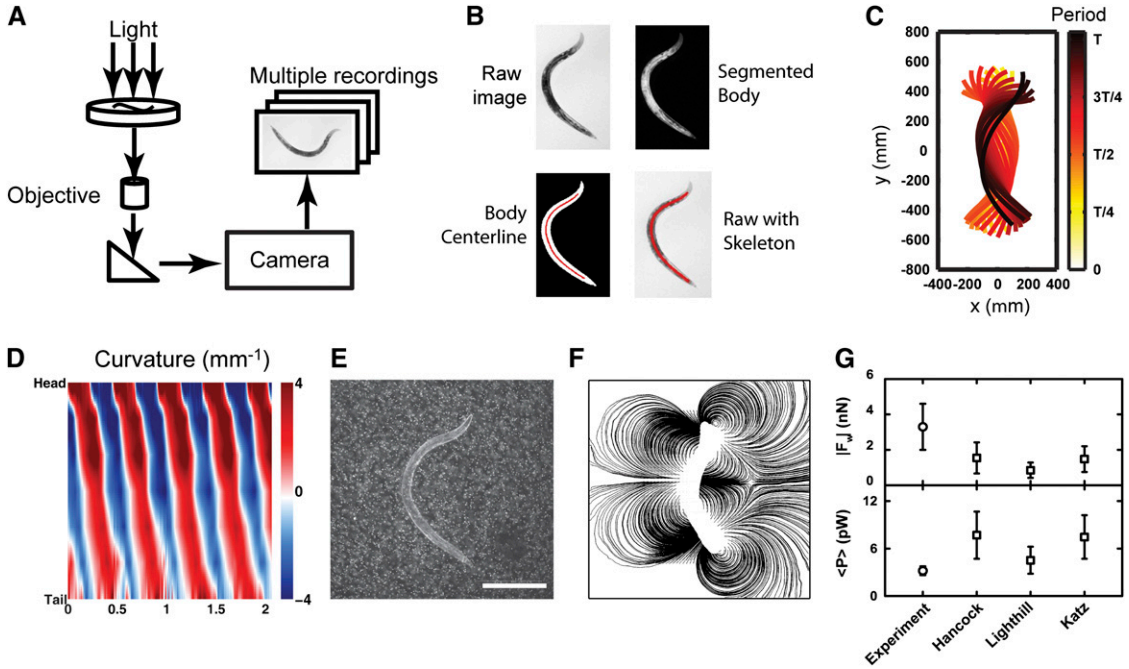

Figure 1 Pipeline for analysis of *C. elegans* biomechanics. (A) Image series are acquired on a standard transmitted light stereo microscope at ≥15 frames per second. Groups of three to five worms were transferred into a 50-μl drop of M9 buffer in the recording chamber and, after 2 min of acclimation, covered with a cover glass (Fisher; catalog no. 12-544-10). (B) TIFF image series were background-subtracted, and the worm was skeletonized. Exported image series were analyzed using our custom algorithms (see File S1 and File S2 for scripts and tutorials) in MATLAB R2010b. To minimize the hydrodynamic boundary effect, recordings in which the nematode touched the top or the bottom of the recording chamber (as determined by a restriction in movement) or was <1 mm away from the chamber boundaries were discarded. To enable background subtraction, the microscope stage was not moved during the recording. Each recording contains a minimum of 4 sec of forward swimming behavior for a single nematode. The spatial pixel resolution was calibrated by imaging a micro-ruler (Electron Microscopy Sciences; catalog no. 62135-01). (C) The envelope of worm skeletons over time, as well as the calculated centroid movement. (D) Nematode's curvature contour plots. (E) Still image of nematode swimming in fluid (density = 1.02 g/cm^3; viscosity = 1 mPa·sec) seeded with 2.2-μm green fluorescent polymer microspheres (Duke Scientific). (Bar, 400 μm). (F) Instantaneous streamlines computed from velocity fields obtained using PTV. Velocities were computed from the local particle displacements (Δs) and the known elapsed times between consecutive frames (Δt). We note that the seeding particles showed negligible Brownian motion compared to the average flow velocity of ~0.5 mm/sec. In support of this, the Péclet number, which is the ratio of the flow-mediated particle movement to the diffusion-mediated particle movement (defined as Pe = *VL*/*D*, where *D* is the diffusion coefficient of the aqueous solution, *V* is the flow average velocity, and *L* is a characteristic length scale) was on the order of 10^6. (G) Magnitudes of the propulsive forces F_{prop} and corresponding power *P* averaged over one beating period. Error bars show standard deviation of the average values. Circles show the experimental values and squares show the theoretical values (Hancock 1953; Katz *et al.* 1975; Lighthill 1976).

Results

The biomechanical features of the *C. elegans* swim gait, such as the propulsion force, mechanical power, and bending modulus, can be estimated by incorporating kinematics data into an elasto-hydrodynamic model (Sznitman J *et al.*, 2010; Sznitman R *et al.*, 2010). We restricted our analysis to the swim gait because biomechanical analysis of the crawling gait is complicated by the presence of lubrication forces, surface tension, and surface rheology. To measure swimming kinematics, we created a MATLAB pipeline for automated image analysis (Figure 1, A–E). Using a standard dissecting microscope and digital camera, we recorded at least eight beating periods of uninterrupted forward locomotion (Figure 1A). The nematode body configurations were segmented and extracted from the background (Figure 1B). Body centroids were computed as the mean positions of the body configuration, and the body centerlines (skeleton composed of 100 points) were obtained from the segmented body configuration via the Augmented Fast Marching Method (Sethian 1996). (Figure 1C). By tracking the body centroids, we calculated the swimming speed (*U*). The nematode undulatory beating behaviors were quantified as a curvature matrix, which contains the temporal and spatial evolution of body curvatures (Figure 1E). The curvature matrix showed a periodic and diagonal pattern, illustrating the propagation of the undulating body wave from head to tail. The undulatory wave speed (*c*), beating period (*T*), swimming frequency ($f = 1/T$) (equivalent to the frequency of "thrashing"), and wavelength ($\boldsymbol{\lambda} = \mathbf{c}\boldsymbol{T}$) quantitatively described the spatio-temporal properties of the body curvature during swimming. Additionally, we obtained several other kinematics features, including bending amplitude at the head, middle, and tail part of the body and the maximum, minimum, and mean body curvatures. The wave efficiency (U/c) and the shape parameter ($\boldsymbol{\lambda}/L$) (Gray and Lissman 1964), which are used to monitor the nematode's motility gait, were derived from the kinematics features. Finally, we incorporated the kinematics data into an elasto-hydrodynamic model (Sznitman J *et al.*, 2010; Sznitman R *et al.*, 2010) to estimate the propulsion forces, mechanical

Table 1 Kinematic and biomechanical properties of wild-type *C. elegans* grown at three cultivation temperatures

Feature category	BMP output	Unit of measurement	N2 16°	N2 20°	N2 25°
Shape	Length	mm	1.1 ± 0.05	1.1 ± 0.05	1.2 ± 0.05
	Body volume	m^3	3.7E-12 ± 3.7E-13	4.0E-12 ± 3.4E-13	5.2E-12 ± 4.4E-13
	Body aspect ratio	N.D.	0.06 ± 0.004	0.06 ± 0.005	0.06 ± 0.004
Kinematics	Swimming speed	mm/sec	0.34 ± 0.07	0.39 ± 0.07	0.34 ± 0.05
	Bending wave speed	mm/sec	3.13 ± 0.5	3.47 ± 0.7	3.65 ± 0.7
	Bending wavelength	mm	1.5 ± 0.2	1.6 ± 0.3	2.0 ± 0.3
	Beating frequency	Hz	2.07 ± 0.1	2.17 ± 0.12	1.82 ± 0.12
	Beating head amplitude	mm	0.2 ± 0.03	0.2 ± 0.03	0.2 ± 0.03
	Beating mid-body amplitude	mm	0.1 ± 0.01	0.1 ± 0.01	0.1 ± 0.02
	Beating tail amplitude	mm	0.2 ± 0.02	0.2 ± 0.02	0.2 ± 0.02
	Maximum curvature	mm^{-1}	9.4 ± 0.9	9.8 ± 1.1	8.2 ± 0.7
	Average curvature	mm^{-1}	4.3 ± 0.3	4.3 ± 0.3	4 ± 0.3
	Minimum curvature	mm^{-1}	2.6 ± 0.3	2.3 ± 0.3	2.6 ± 0.3
Dynamics	Bending force	nN	1.2 ± 0.2	1.3 ± 0.2	1.1 ± 0.2
	Mechanical power	pW	3.6 ± 0.6	4.4 ± 1.1	3.5 ± 0.7
Material properties	Relative bending modulus	Nm^2	1.6E-14 ± 6.7E-15	1.9E-14 ± 8.8E-15	2.5E-14 ± 1.2E-14
Efficiency	U/c (speed/wave speed)	N.D.	0.11 ± 0.02	0.11 ± 0.02	0.1 ± 0.02
	Λ/L (wavelength/length)	N.D.	1.43 ± 0.18	1.48 ± 0.23	1.69 ± 0.33

N.D., non-dimensional measurement.

power, and a relative bending modulus of the nematode body. The relative bending modulus is derived by assuming a particular equation to describe the preferred curvature waveform (Sznitman J *et al.*, 2010) for the active moment. Although our preferred waveform equation accommodates key features of the swim gait (curvature propagation is sinusoidal, phase differences exist along the length of the animal, and the curvature amplitude at the head is greater than at the tail), other descriptions of the waveform are possible and would yield different estimates of the material properties. However, such equations could be solved only by using numerical simulations, which would introduce additional uncertainties. Our solution allows us to eliminate the waveform from our equations of motion and calculate a relative bending modulus, $K_{b,}$ without numerical simulations (for a more detailed description, see Sznitman J *et al.*, 2010). Overall, this analysis provides 18 quantitative features that describe periodic averages and spatio-temporal features of the wild-type swim gait (Table 1).

Our approach for the quantification of the swim gait was based on the classical hydrodynamic model, *i.e.*, resistive force theory (Hancock 1953; Gray and Hancock1955), which linearly relates the hydrodynamic drag force to the locomotion speed, and slender body theory (Lighthill 1976; Johnson 1979). For a free swimmer, the drag force, F_{drag}, experienced by the nematode is balanced by the propulsion force, F_{prop}, such that $F_{\mathrm{drag}} + F_{\mathrm{prop}} = 0$; therefore, the nematode propulsion force is simply $-F_{\mathrm{drag}}$. Resistive force theory can be used to estimate the drag force F_{drag} once the drag coefficients are determined. To further validate this approach, we also sought to experimentally validate these calculations by measuring the fluid stresses acting on the nematode by measuring the velocity fields produced by nematodes swimming in a fluid of known viscosity (μ) using particle tracking velocimetry (PTV). In PTV, small (2.2μ) fluorescent beads are added to the swimming media (liquid). The vector and velocity of individual particles is proportional to their distance from the nematode as well as to the applied local force generated by the swimming nematode. Using PTV, we resolved a high resolution and dynamic velocity field, V, of the fluid (Figure 1G). The shear rate of the flow is $\dot{\boldsymbol{\gamma}} = \mathbf{1/2}(\nabla \boldsymbol{V} + \nabla \boldsymbol{V}^T)$, where $\nabla \boldsymbol{V}$ is the spatial gradient of the velocity field. The total hydrodynamic drag force on the nematode was computed as $\boldsymbol{F_{drag}} = \int_{Sw} \boldsymbol{\mu}\ \dot{\boldsymbol{\gamma}}\ \boldsymbol{dS}$, where $\boldsymbol{\mu}$ is the viscosity of the fluid (∼1.0 mPa·sec for M9 buffer solution), and the drag force was obtained by integrating over the entire body surface, S_w. The corresponding mechanical power was defined as $\boldsymbol{P} = -\int_{Sw}(\boldsymbol{\mu}\ \dot{\boldsymbol{\gamma}}) \cdot \boldsymbol{V}\ \boldsymbol{dS}$. Thus, the integrated drag force and mechanical power were obtained at each instant of the swimming cycle. We found that the experimentally measured propulsion force and mechanical power generated by PTV were highly similar to estimations from the hydrodynamic model (Hancock 1953; Gray and Hancock 1955; Lighthill 1976; Johnson 1979) (Figure 1G). Therefore, two independent measures of nematode swimming biomechanics, PTV and resistive force theory, provide similar quantitative estimates of nematode biomechanics.

To make our integrated platform accessible to all users regardless of computational background, we derived a simple graphical user interface for automated analysis of swimming movies. After defining the location of a family of sequentially named .tif images (multiple independent recordings can be analyzed and summary statistics are reported), the acquisition parameters, such as spatial resolution (μ/pixel) and recording speed (frames per second), are entered. For each movie series, the background-subtracted skeletonized body images are shown. Users can adjust body and skeleton threshold values to obtain the best fit to their recording conditions. After definition, users see the progress of analysis, including summary kinematics, biomechanics, skeletonization, and curvature plots. Upon completion of the analysis, summary statistics for each of the 18 parameters are shown and users can

review each individual recording for accuracy using trajectory plots, curvature analysis, and/or a skeleton browser. Confounding data (*i.e.*, reversals and omega turns) can be cropped from the recording within the curvature window. After cropping, recordings are reanalyzed, and the summary statistics are updated. Data are output as .txt files for further analysis.

Using this automated BMP pipeline, we analyzed the phenotypic properties of several well-described mutants affecting neuromuscular structure/function (Figure 2). A surprising feature of many such mutants is the failure of a null allele to produce a visually apparent defect in the motility gait. We wanted to determine if automated BMP might provide a more sensitive metric for detecting motility defects in such mutants. Previous studies utilizing a simple measurement of motility, thrashing (equivalent to the frequency measurement in our analysis), has revealed phenotypic defects in many mutants. The BMP method also detected such defects (*dys-1*, *lev-10*, *unc-29*, etc., in Figure 2A). However, several mutants affecting important components of the synaptic or muscle machinery exhibited insignificant defects in swim frequency. Using other BMP parameters, we were able to define phenotypic defects in these mutants that did not manifest as defects in swim frequency. For example, *ace-1* and *ace-2* mutants, which affect acetylcholinesterase subunits, exhibit normal swim frequency. However, both swim with significantly reduced speed (Figure 2B). Moreover, *ace-1* can be differentiated from *ace-2* in that *ace-1* shows a defect in body curvature kinematics (Figure 2C), while *ace-2* produces less swim power (Figure 2D). Similarly, *lev-11*, which encodes a tropomyosin homolog, exhibits normal frequency, speed, and power (Figure 2, A, B, and D) but shows a defect in body curvature kinematics (Figure 2C). Finally, mutations in *sgn-1*, which encodes a *C. elegans* sarcoglycan homolog, give rise to animals with normal swim frequency (Figure 2A) but defective swim speed (Figure 2B) and power (Figure 2D). These examples demonstrate the utility of BMP for detecting novel motility phenotypes on the basis of simple video recording, automated image analysis, and applied fluid mechanics approaches.

While the analysis of individual kinematic and biomechanical parameters is a useful application of BMP, we also consider the possibility that the pattern of BMP parameters may also be informative. Specifically, we hypothesized that BMP could provide a phenotypic profile that is predictive of gene function, much like gene expression across a range of conditions can be predictive of gene function (Kim *et al.* 2001). To test this hypothesis, we utilized BMP to analyze a group of 21 well-characterized mutant strains affecting known aspects of neuromuscular function (Table S1). Following normalization of mean quantitative BMP parameters to the wild-type strain, we clustered the biomechanical profile using standard hierarchical clustering (Saeed *et al.* 2003). From this analysis, two phenotypic clusters were evident among the 21 mutants analyzed (Figure 3A, red and

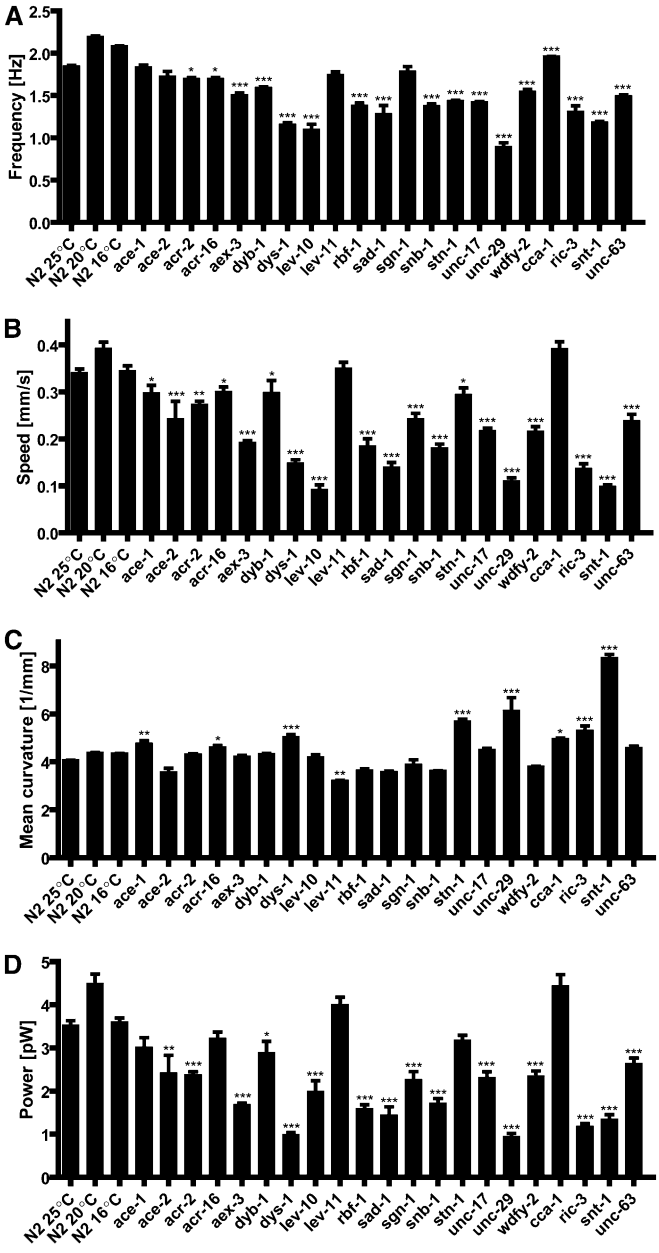

Figure 2 Selected kinematic and biomechanical properties of locomotion captured by BMP. Bar graphs representing BMP software-calculated (A) frequency (Hz), (B) speed (mm/sec), (C) mean curvature (1/mm), and (D) mechanical power (pW). Data shown are means ± SD, ≥10 animals per genotype were recorded as described for Figure 1, and the population averages for each parameter were compared statistically with one-way ANOVA followed by Bonferroni's Multiple Comparison Test for significance. $*P < 0.05$; $**P < 0.01$; $***P < 0.001$. All strains were maintained on standard NGM agar plates and fed with the *Escherichia coli* strain OP50. Analysis was performed on hypochlorite-synchronized young adult animals of the following strains grown at the indicated temperature: 25°: wild type (N2, Bristol), VC505 *ace-1(ok663)*, GG202 *ace-2(g72)*, RB1559 *acr-2(ok1887)*, RB918 *acr-16(ok789)*, NM2739 *aex-3(js815)*, LS505 *dyb-1(cx36)*, LS292 *dys-1(cx18)*, ZZ17 *lev-10(x17)*, ZZ12 *lev-11(x12)*, NM1278 *rbf-1(js232)*, CX5156 *sad-1 (ky289)*, RB1882 *sgn-1(ok2432)*, NM534 *snb-1(js17)*, LS721 *stn-1(ok292)*, CB933 *unc-17(e245)*, CB1072 *unc-29(e1072)*, and RB2580 *wdfy-2 (ok3592)*; 20°: wild type (N2, Bristol), JD21 *cca-1(ad1650)*, RM509 *ric-3 (md158)*, NM204 *snt-1(md290)*, and ZZ26 *unc-63(x26)*. Wild-type nematodes grown at the appropriate temperature were used as controls.

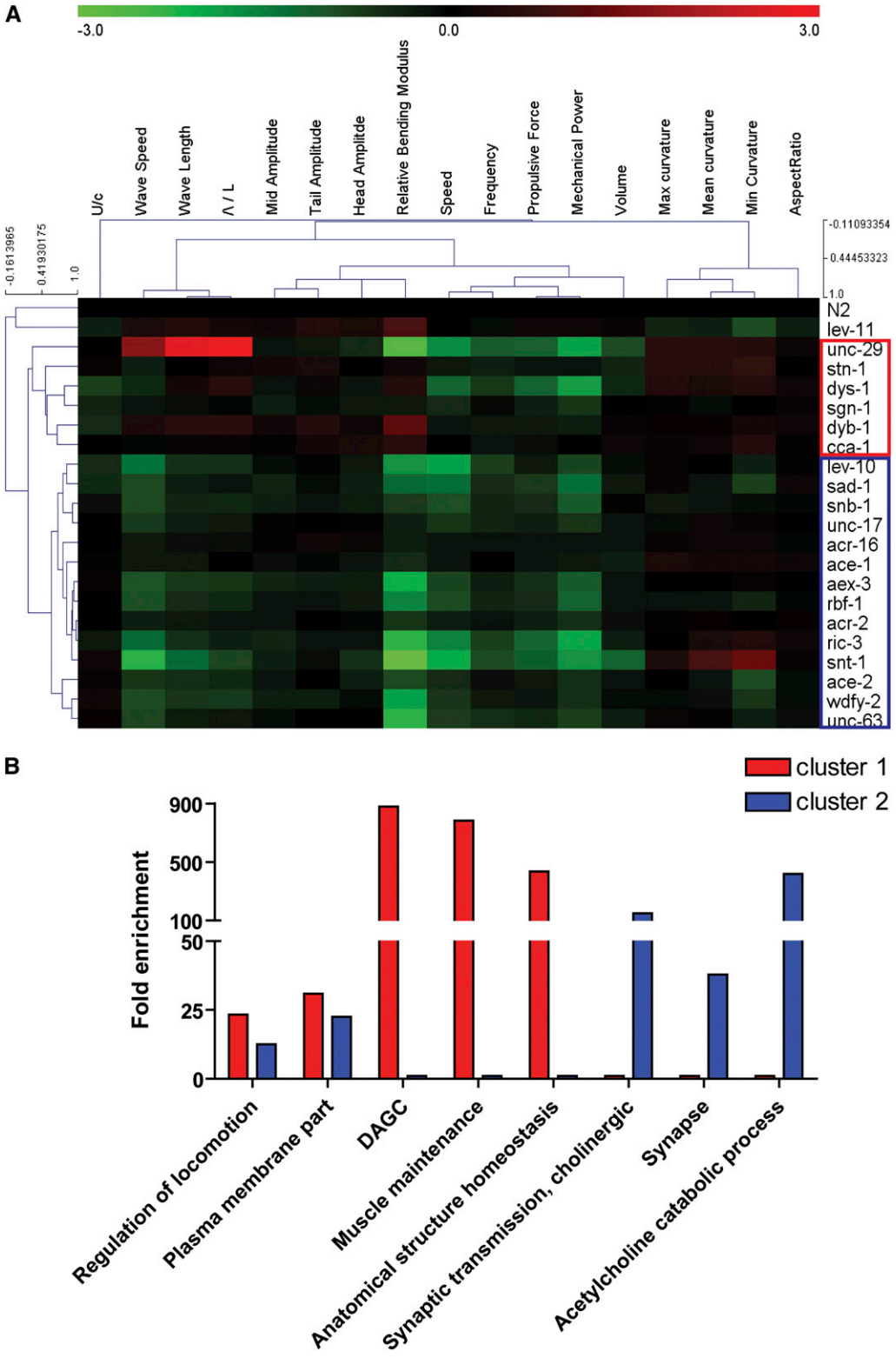

Figure 3 Biomechanical profiling of synaptic mutants is predictive of gene function. (A) Hierarchical clustering of biomechanical phenotypes and mechanical features of 21 well-characterized synaptic mutant strains. Blue outline: cluster 1; red outline: cluster 2. Prior to clustering, each biomechanical parameter was normalized to the relevant temperature-matched wild-type control parameter. Log2-transformed data were clustered using the hierarchical clustering method, as implemented in the TM4 Microarray Software Suite (Saeed *et al.* 2003). We note that the accuracy of clustering depends on the inclusion of the modeled relative bending modulus parameter. Omission of this parameter results in substantially less robust functional clustering. However, the relative bending modulus parameter alone is not sufficient to functionally cluster genes (data not shown). (B) DAVID functional annotation tool enrichment scores for cluster 1 (red) and cluster 2 (blue). Bar graphs representing fold enrichment of functional annotation clustering. Genes from each of the two clusters shown in A were individually analyzed for Gene Ontology enrichment using the DAVID web tool (http://david.abcc.ncifcrf.gov/). Functional categories with false-discovery rates of <1% were taken to indicate that the functional category was significantly enriched, as compared to the *C. elegans* genome at large.

blue outlines). Within the clusters, we noted that several genes exhibited related functions. For example, *dys-1* mutants robustly clustered with *sgn-1* and *dyb-1* mutants. *dys-1* (dystrophin), *sgn-1* (sarcoglycan), and *dyb-1* (dystrobrevin) encode protein components of the dystrophin-associated glycoprotein complex (DAGC), which links the cytoskeleton to the extracellular matrix in muscles. Since almost all genes in cluster 1 are components of the same protein complex, this cluster may correspond to genes that, when mutated, destabilize DAGC. Similarly, cluster 2 is primarily composed of genes involved in acetylcholine signaling, such as *acr-16* and *unc-63* (AChR subunits) (Culetto *et al.* 2004; Touroutine *et al.*

2005), *ace-1* and *ace-2* (acetylcholinesterases) (Combes *et al.* 2001), and *lev-10* (AChR clustering) (Gally *et al.* 2004). Analysis of the BMP clusters using the functional annotation tool DAVID (Huang da *et al.* 2007) confirmed that genes in cluster 1 are significantly enriched for DAGC gene ontology (GO) categories while those in cluster 2 are enriched for cholinergic-signaling GO categories (Figure 3B). These data show that BMP-based clusters are significantly enriched for functionally related genes and, within this limited set of data, are predictive of gene function.

We have developed a free, user-friendly, and quantitative solution for integrative analysis of *C. elegans* locomotion. Our method uses equipment commonly found in *C. elegans* research labs, making it easy and inexpensive to implement. Previous studies have used manual approaches to report widely varying model-independent features of the swim gait (*i.e.*, swim frequency of 1.6–4.0 Hz). Our data fall within this range and agree well with other recent automated analyses of the swim gait performed with independently generated software [frequency: 2.2 ± 0.1 Hz (our data) *vs*. 1.76 ± 0.1 Hz (Fang-Yen *et al.* 2011); λ/L: 1.48 ± 0.23 (our data) *vs.* 1.54 ± 0.04 (Fang-Yen *et al.* 2011)]. However, we note that our model-based estimates of nematode relative bending modulus differ from previous reports (Fang-Yen *et al.* 2011). This discrepancy likely results from differences in experimental methods, *i.e.*, free-swimming animals (our approach) *vs.* restrained and bent animals (Fang-Yen *et al.*'s approach), even though similar mathematical methods are used. Even when using these different approaches, we note that the estimated bending moduli are of the same order of magnitude (10^{-14} N/m^2) and differ by only fivefold. Therefore, BMP exhibits a high degree of similarity with previous studies of *C. elegans* kinematics, hydrodynamics, and biomechanics. As new data or modeling approaches become available, our MATLAB code could be easily modified to accommodate these changes and improve the accuracy of BMP.

Although the resulting data are high content, they are inherently low throughput. A natural extension of this approach would be to adopt its use within a more high-throughput context, such as a microfluidics or a multiwell plate format. Currently, such high-throughput screens in *C. elegans* are limited to a single endpoint (*i.e.*, paralysis) (Kwok *et al.* 2006) or death (Petrascheck *et al.* 2007). Screens that provide more detailed phenotypic discrimination would allow the identification of small molecules that exert more specific or subtle effects on locomotion phenotypes caused by either endogenous genetic mutations or transgene-based disease models. BMP will also complement other existing platforms, such as the parallel worm tracker (Ramot *et al.* 2008) and the multi-worm tracker (Swierczek *et al.* 2011), which analyze more complex motility gaits that are not compatible with BMP analysis. In conclusion, we have developed an integrated algorithm to quantitatively describe the biomechanics of the *C. elegans* swim gait. The BMP approach should be of tremendous benefit to the community of *C. elegans* researchers and will make phenotypic analyses more standardized, quantitative, accurate, and robust.

Acknowledgments

We acknowledge the National Bioresource Project for providing some *C. elegans* strains. This work was supported by a grant from the Muscular Dystrophy Association (T.L.), National Institutes of Health (NIH) grant R21NS065936 (T.L.), National Science Foundation grant (NSF)-CBET-CAREER-0954084 (P.A.), and NSF grant CMMI 1066787 (P.K.P.). Some nematode strains used in this work were provided by the *Caenorhabditis* Genetics Center, which is funded by the NIH National Center for Research Resources.

Literature Cited

Brenner, S., 1974 The genetics of *Caenorhabditis elegans*. Genetics 77: 71–94.

Buckingham, S. D., and D. B. Sattelle, 2009 Fast, automated measurement of nematode swimming (thrashing) without morphometry. BMC Neurosci. 10: 84.

Combes, D., Y. Fedon, J. P. Toutant, and M. Arpagaus, 2001 Acetylcholinesterase genes in the nematode Caenorhabditis elegans. Int. Rev. Cytol. 209: 207–239.

Culetto, E., H. A. Baylis, J. E. Richmond, A. K. Jones, J. T. Fleming *et al.*, 2004 The Caenorhabditis elegans unc-63 gene encodes a levamisole-sensitive nicotinic acetylcholine receptor alpha subunit. J. Biol. Chem. 279: 42476–42483.

Fang-Yen, C., M. Wyart, J. Xie, R. Kawai, T. Kodger *et al.*, 2011 Biomechanical analysis of gait adaptation in the nematode Caenorhabditis elegans. Proc. Natl. Acad. Sci. USA 107: 20323–20328.

Gally, C., S. Eimer, J. E. Richmond, and J. L. Bessereau, 2004 A transmembrane protein required for acetylcholine receptor clustering in Caenorhabditis elegans. Nature 431: 578–582.

Gray, J., and G. Hancock, 1955 The propulsion of sea-urchin spermatozoa. J. Exp. Biol. 32: 802–814.

Gray, J., and H. W. Lissman, 1964 The locomotion of nematodes. J. Exp. Biol. 41: 135–154.

Hancock, G. J., 1953 The self-propulsion of microscopic organisms through liquids. Proc. R. Soc. Lond. (A) Math. Phys. Sci. 217: 96–121.

Huang da, , W., B. T. Sherman, Q. Tan, J. Kir, D. Liu *et al.*, 2007 DAVID Bioinformatics Resources: expanded annotation database and novel algorithms to better extract biology from large gene lists. Nucleic Acids Res. 35: W169–W175.

Johnson, B. E., 1979 An improved slender-body theory for Stokes flow. J. Fluid Mech. 99: 411–431.

Katz, D. F., J. R. Blake, and S. L. Paverifontana, 1975 Movement of slender bodies near plane boundaries at low Reynolds-number. J. Fluid Mech. 72: 529–540.

Kim, S. K., J. Lund, M. Kiraly, K. Duke, M. Jiang *et al.*, 2001 A gene expression map for Caenorhabditis elegans. Science 293: 2087–2092.

Kwok, T. C., N. Ricker, R. Fraser, A. W. Chan, A. Burns *et al.*, 2006 A small-molecule screen in C. elegans yields a new calcium channel antagonist. Nature 441: 91–95.

Lighthill, J., 1976 Flagellar hydrodynamics. SIAM Rev. Soc. Ind. Appl. Math. 18: 161–230.

Nahabedian, J. F., H. Qadota, J. N. Stirman, H. Lu, and G. M. Benian, 2011 Bending amplitude—a new quantitative assay of C. elegans locomotion: identification of phenotypes for mu-

tants in genes encoding muscle focal adhesion components. Methods 56: 95–102.
Petrascheck, M., X. Ye, and L. B. Buck, 2007 An antidepressant that extends lifespan in adult Caenorhabditis elegans. Nature 450: 553–556.
Pierce-Shimomura, J. T., B. L. Chen, J. J. Mun, R. Ho, R. Sarkis *et al.*, 2008 Genetic analysis of crawling and swimming locomotory patterns in C. elegans. Proc. Natl. Acad. Sci. USA 105: 20982–20987.
Ramot, D., B. E. Johnson, T. L. Berry Jr., L. Carnell, and M. B. Goodman, 2008 The Parallel Worm Tracker: a platform for measuring average speed and drug-induced paralysis in nematodes. PLoS ONE 3: e2208.
Saeed, A. I., V. Sharov, J. White, J. Li, W. Liang *et al.*, 2003 TM4: a free, open-source system for microarray data management and analysis. Biotechniques 34: 374–378.
Sethian, J. A., 1996 A fast marching level set method for monotonically advancing fronts. Proc. Natl. Acad. Sci. USA 93: 1591–1595.
Swierczek, N. A., A. C. Giles, C. H. Rankin, and R. A. Kerr, 2011 High-throughput behavioral analysis in C. elegans. Nat. Methods 8: 592–598.
Sznitman, J., P. K. Purohit, P. Krajacic, T. Lamitina, and P. E. Arratia, 2010 Material properties of Caenorhabditis elegans swimming at low Reynolds number. Biophys. J. 98: 617–626.
Sznitman, R., M. Gupta, G. D. Hager, P. E. Arratia, and J. Sznitman, 2010 Multi-environment model estimation for motility analysis of Caenorhabditis elegans. PLoS ONE 5: e11631.
Touroutine, D., R. M. Fox, S. E. Von Stetina, A. Burdina, D. M. Miller III *et al.*, 2005 acr-16 encodes an essential subunit of the levamisole-resistant nicotinic receptor at the Caenorhabditis elegans neuromuscular junction. J. Biol. Chem. 280: 27013–27021.
Tsechpenakis, G., L. Bianchi, D. Metaxas, and M. Driscoll, 2008 A novel computational approach for simultaneous tracking and feature extraction of C. elegans populations in fluid environments. IEEE Trans. Biomed. Eng. 55: 1539–1549.

Communicating editor: O. Hobert

GENETICS

Supporting Information
http://www.genetics.org/content/suppl/2012/05/02/genetics.112.141176.DC1

Biomechanical Profiling of *Caenorhabditis elegans* Motility

Predrag Krajacic, Xiaoning Shen, Prashant K. Purohit, Paulo Arratia, and Todd Lamitina

DOI: 10.1534/genetics.112.141176

Table S1 and File S1

Table S1 contains all supporting data. File S1 contains the BMP MATLAB code, Sample data - wt worm 1-5, and instructions for Matlab program.

All files are available for download at http://www.genetics.org/content/suppl/2012/05/02/genetics.112.141176.DC1.